An EUV spectrometer for mapping the heliopause and solar wind

M.Lampton[a], J.Edelstein[a], T.Miller[b], M.Gruntman[c]

[a]Space Sciences Lab, University of California, Berkeley CA 94720 USA
[b]T-Stop Design, El Cerrito CA 94530 USA
[c]Astronautics and Space Technology Division, Viterbi School of Engineering,
University of Southern California, Los Angeles CA 90089 USA

ABSTRACT

The He+ ion provides a valuable tracer of solar wind dynamics and the heliospheric boundary. Mapping the heliosphere in the 30.4 nm resonance line of the He+ ion with high spectral resolution will open access to the heliopause and reveal the three-dimensional flow of the solar wind. The emission fluxes are however faint, just a few mR, which poses a serious limitation on the mapping rate at high signal-to-noise ratio. We have developed a spectrometer configuration for narrowband EUV emission that offers important advantages over previous designs: high throughput (~1cps/mR), high resolution (several thousand), no moving parts, and modest instrument size and mass. The concept combines a conventional normal-incidence Rowland mount grating and an efficient multilayer coating, with a microchannel plate detector performing two dimensional photon counting. One key innovation is the use of a large-area multi-slit at the spectrometer entrance. This multislit is a one dimensional sequence of open and opaque zones, against which pattern the accumulated spectral image can be correlated to recover the incident spectrum. The other innovation is arranging that each member of the multislit group is curved in such a way that the off-plane grating aberrations (which extend and rotate the image of each object point) do not introduce significant wavelength broadening. The curved slit arrangement yields a large well-corrected image field, and a high throughput for diffuse emission is achieved. The curved-multislit Rowland spectrometer may have a variety of other applications sensing diffuse fluxes with high spectral resolution.

Keywords: heliosphere, heliopause, solar wind

1. INTRODUCTION

Imaging of the global heliosphere in EUV with high spectral resolution is emerging as a highly promising experimental tool that will probe the distant galactic frontier of the solar system[1-3]. This is the region where the expanding solar wind plasma meets the surrounding interstellar plasma. The boundary separating solar and interstellar matter, the heliopause, is believed to be at 150-200 AU from the sun. The heliosphere and its boundary are essentially asymmetric which calls for remote sensing to establish its properties. The measurement of the glow of interstellar plasma flowing around the heliopause will reveal the shape of the heliopause and probe the ionization state of the LISM. The most promising radiation is expected at He+ line 30.4 nm, with the estimated radiance a few milli-Rayleigh. (1 R = 1 Rayleigh = $10^6/4\pi$ phot cm^{-2} s^{-1} sr^{-1}.) Other emission processes from the He+ ion are charge exchange from solar wind alpha particles on interplanetary hydrogen, and hot plasma within the interstellar Local Bubble contribute at comparable intensity[1-3] but are Doppler shifted, providing unique spectroscopic signatures of these processes.

To map these emissions requires a spaceborne instrument with milli-Rayleigh sensitivity for diffuse EUV near 30.4nm in time scales of 1000-10000 seconds (angular bins 5°×5°) and spectral resolution 0.005 nm, a combination of features that cannot be obtained with conventional spectrometers. In the accompanying paper[3] we describe the science rationale, the mission, and the aperture coding arrangement. In this paper, we describe the coded-aperture spectrometer optical system, and show results of lab tests with a visible-wavelength analog of the planned EUV instrument.

Author information: mlampton@SSL.berkeley.edu

UV, X-Ray, and Gamma-Ray Space Instrumentation for Astronomy XIV
edited by Oswald H. W. Siegmund, Proc. of SPIE Vol. 5898
589810, (2005) · 0277-786X/05/$15 · doi: 10.1117/12.615553

2. THE UNCOMPENSATED ROWLAND SPECTROMETER

The traditional Rowland spectrometer mount (Rowland[4]) comprises an entrance slit, a concave diffraction grating, and an image sensor. Its imaging properties have been described by Beutler[5] and Namioka[6]. For a general treatments see Spencer and Murty[7] whose right-handed coordinate system we adopt here, and Neviere et al[8].

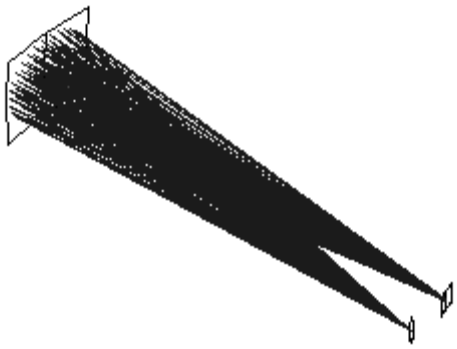

Figure 1: Schematic illustration of the Rowland spectrometer geometry. The origin of the coordinate system is at the center of the ruled grating face. The Z axis is the grating normal and the Y axis lies along the groove direction, vertically upward in this figure. The +X is the direction of dispersion for positive orders. A narrow slit is shown on the normal and a rectangular detector is shown to the +X side of the normal.

The radius of curvature of the spherically concave grating equals the diameter D of the Rowland circle in the XZ plane, tangent to the grating surface. A point source on the Rowland circle has coordinates [Dsinα cosα, 0, D $\cos^2\alpha$] where α is the angle of incidence onto the grating center. The first order diffracted light arrives in spectral focus at another point on the Rowland circle [D sinβ cosβ, 0, D$\cos^2\beta$] where the angle of diffraction β obeys

$$\sin\alpha + \sin\beta = mg\lambda \qquad (1)$$

with groove density g, spectral order m, and wavelength λ. The remarkable fact responsible for the continuing popularity of the Rowland mount is that it delivers an excellent spectrum focus at all object and image points along the Rowland circle, even for a usefully large beam opening angle. Moreover, no additional focusing or collimating optics are needed to obtain this spectrum. These advantages invite its use for applications in the extreme ultraviolet where refracting materials are nonexistent and reflectors have rather poor reflectivity**.**

The dominant aberration for the Rowland mount is astigmatism. For nonzero α or β, the vertical focus departs from the spectrum focus, so that the diffracted image of an in-plane source point becomes a narrow vertical line, parallel to the grating grooves, extending above and below the Rowland circle. To lowest order in α and β, the end-to-end height of the astigmatic arc seen in the image is given by

$$\Delta Y = L(\alpha^2 + \beta^2) \qquad (2)$$

where L is the length of a grating groove.

If the illuminating source is extended to become a short vertical slit, the chief consequence is to extend the height of this image line, again without any first order impact on the spectral resolution.

Multiple entrance slits can be disposed along the Rowland circle and will of course give multiple line images along the Rowland circle. For a single line with complex Doppler structure such as the heliospheric 30.4 He+ group, multiple

end-to-end spectra can then be obtained in parallel. Further multiplicity and hence throughput can be achieved by packing these slits into a 50% average pattern of open and blocked slits that constitute a binary orthogonal sequence. Although the subspectra overlap, and an individual photon's wavelength cannot be distinguished, the source spectrum can be decoded from an accumulated image by cross correlating the image with the known slit pattern[3].

3. THROUGHPUT

The throughput of such an instrument demands slit height as well as a large number of slits. The overall effective etendue E of the spectrometer working near normal incidence is given by

$$E = A \bullet \Omega \bullet R \bullet B \qquad (3)$$

where the A is the aggregate area H•W•N of the N slits each of height H and width W, Ω represents the solid angle of light that illuminates the grating (essentially the inverse square of the f/number), R is the grating reflectance, and B represents the grating groove blaze efficiency.

In this picture the resolution requirement serves to fix one constraint on the spectrometer system. Let the detector resolution be some given linear dimension "d". Then the slit width W must be chosen to be of this same order, W~d. Since the linear dispersion near normal incidence is $dx/d\lambda = D \bullet m \bullet g$, it follows that this D•m•g product is immediately fixed by the system linear resolution and the required wavelength resolution.

D is constrained by (and indeed determines) the overall instrument length, while diffraction order m=1 is preferred for best groove efficiency in the far or extreme UV, and the groove density is limited by current manufacturing capabilities to values around 6000 grooves/mm. The spectral resolving power $R = \lambda/d\lambda = S/d$ where S is the linear separation distance between zero order and first order images.

The factors that remain available for boosting throughput are the size of the instrument governed by D, and by the height H and number N of the individual slits. Whereas D drives the size and cost of the grating, the payload, and the mission mass, H and N are relatively cheap to increase: H merely feeds the grating with a larger range of incident angles above and below the grating plane of diffraction, while N impacts only the free spectral range. The CHIPS spectrometer[9] and the IMAGE FUV experiment[10,11] have used multiple slits to achieve improved throughputs.

With nonzero H the grating is illuminated from off-plane points. The off-plane aberrations of the concave grating are not zero. As a point source moves off-plane to a height Y above the Rowland circle, it illuminates the grating at an elevation angle γ=Y/D and its astigmatically-stretched image rotates as it moves off-plane. To first order in α, β, and γ, the end-to-end horizontal extent of its astigmatic arc is given by

$$\Delta X = L\, \gamma\, (\alpha - \beta). \qquad (4)$$

The slope of this arc in image coordinates is then

$$\Delta X/\Delta Y = \gamma\, (\alpha - \beta) / (\alpha^2 + \beta^2) \qquad (5)$$

Figure 2 below illustrates the magnitude of this off-plane rotation for a D=1meter spectrograph whose entrance slit has been replaced by a grid of points spanning a zone 4cm x 4cm a centered on the grating normal. For this and the following examples, $m \bullet g \bullet \lambda = 0.10944$ and $\beta = 6°.283$ appropriate for 30.4nm radiation and g=3600/mm rulings. What is clear from this figure is that individual object points lying off the plane of diffraction yield images that are stretched vertically, and (more seriously) also are somewhat rotated into the dispersion direction. If uncompensated, this rotation would broaden any spectral line into a bow tie figure and seriously limit the grating's ability to deliver large throughput (needing a large object area) and a high resolution (needing a small object area). The spectral width of lines broadened

in this way would be proportional to the slit height H. If multiple slits were to be employed without correcting for this rotation, the bow tie patterns would overlap, imposing a severe limit to the allowable density of multiple slits.

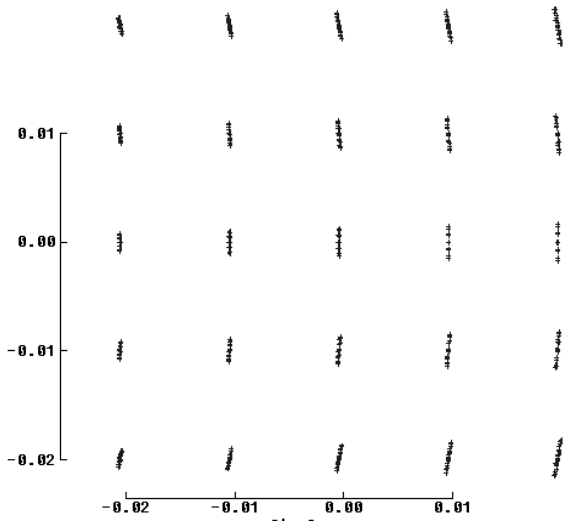

Figure 2: **The problem**: a dispersed image of a monochromatic square 5x5 grid of point sources situated around the point [0,0,D] extending ±20 mm in X and Y. The astigmatism extends each point vertically by 2 to 3mm, and the off-plane conical diffraction rotates each line away from the vertical, with ΔX ranging up to 0.5mm. If the input slits were straight, as usual, the spectra would be broadened by this rotation. Coordinates are in meters.

4. CURVED ENTRANCE SLITS

If however the multiple slits at the entrance plane were curved in the XY plane, so that the image locus followed the off-plane line rotation slope, then the amount of rotation (and height) would not broaden the spectral signatures to first order. Second order broadening remains, since the short segments do not perfectly conform to the curved locus. However, working near the grating normal where both α and β are small, this astigmatic height is given by $h = L(\alpha\text{^}2 + \beta\text{^}2)$ to first order (Beutler[5]). In our case, the resulting second order broadening is far smaller than the first order bow-tie width. To lowest order, the entrance slit equation

$$X(Y) = - Y^2 (\alpha - \beta) / 2D(\alpha^2 + \beta^2) \qquad (6)$$

curves its first order spectrum in such a way as to follow the off-plane astigmatism. For a given spectral resolution, such a curved slit allows a remarkable increase in slit farm height H and thus in system throughput. For the central slit position in the example shown in Figure 2, this first-order formula suggests that, for our example spectrometer, the slits should be curved according to $Y=AX^2$ with A=+4.5687 and X,Y in meters, giving a total deviation in Y of 1.8mm towards the first order image at the top and bottom of our 40mm tall field.

5. HORIZONTAL AND VERTICAL FOCUSING

In addition to the slits being curved within the slit plane, it is of course important to maintain accurate spectrum focus. In the nominal Rowland geometry, focus is achieved by conforming the source and the detector to the Rowland circle. Common photon counting image detectors are however flat and are therefore unable to achieve good focus over a wide image field produced by the Rowland mount. For a narrow line group, however, this is not a problem: each object point has a definite zone on the detector where its short spectrum needs to be focussed. By curving the slit farm into a cylinder whose axis is parallel to the grating grooves, the object location can focus its image onto the flat detector. The slit farm should, to lowest order, bend towards the grating with twice the horizontal (XZ plane) curvature that the Rowland circle has.

In addition to the slits being curved in the slit plane and in the horizontal plane, it is also important that they be focused in the vertical YZ plane. Rather than study the slit curvature optimization using analytic expansions of the ray path differences in powers of the angles, we performed the work numerically using exact vector ray tracing. The general vector grating diffraction equation of Spencer and Murty[7] was implemented in the Java language, and a Levenberg-Marquardt-Lampton optimizer[12] was used to explore a space of three dimensional entrance slit loci.

We confirm that the low order formulas described above yield significant improvements in resolution compared with the simple straight slit case: the slit cylinder whose X curvature = +4 (twice the Rowland cylinder curvature) and the in-plane slit curve coefficient "A" above yield an RMS error of 41 microns in the image X direction, when averaged over a 5 x 5 grid of point source locations with 37 ray directions sampling each grid point. The only optimizations in this first run were for slit piston, image offset, and image demagnification.

Allowing numerical optimization of some remaining slit parameters yields a further substantial improvement over the first-order prediction. Freeing up the horizontal curvature of the slit array, and also allowing the its vertical profile to be curved, reduces the X axis error to 12 microns RMS. The best fit curvature is +3.63 in X and +1.88 in Y. Both curvatures are towards the grating; the slit farm is therefore toric.

We confirm numerically that the parabolic entrance slit formula (6) is close to optimum, and also discovered that there is a further small resolution improvement achieved by allowing the "A" coefficient vary slightly over the horizontal extent of the entrance slit zone. It is best fit with a smooth quadratic function of the X intercept of the slit. The best fit A(X) function is $A(X)=+4.72-840X^2Y^2$ for the slit, and $-4.72+677X^2Y^2$ for the image fit function (X,Y in meters). Averaged over the field, the resulting X fit error is reduced to 8 microns RMS.

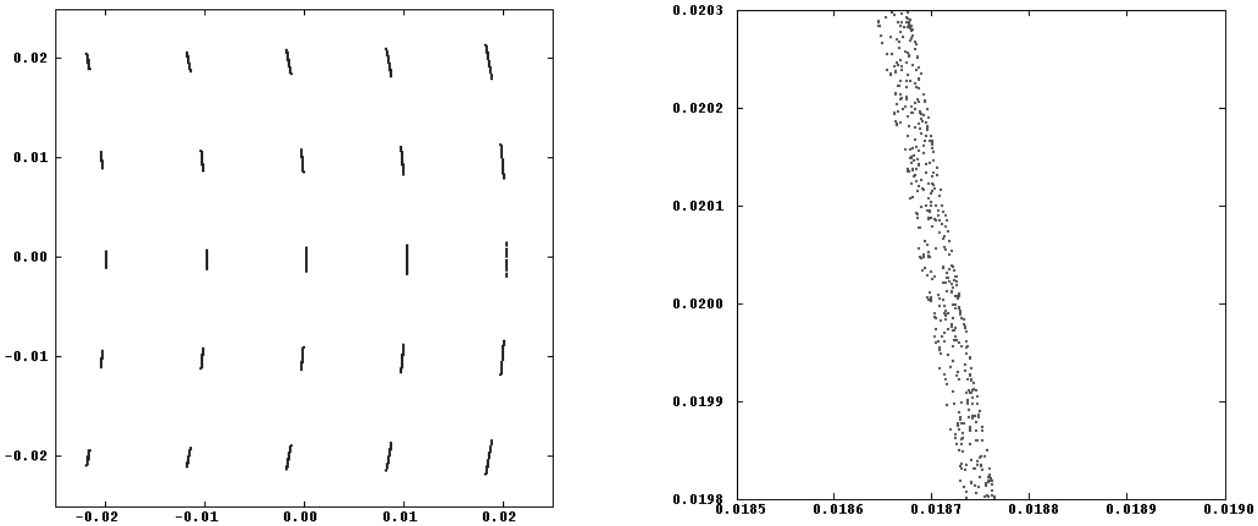

Fig.3: **The solution.** Left: diffracted spot pattern originating from a 5x5 grid of monochromatic point sources located along curved vertical arcs as described in the text. Right: enlargement of diffracted light from a densely populated arc of monochromatic points in the upper right corner of the field; tick marks are spaced 100 microns showing narrowness of each spectrum feature. Coordinate values are shown in meters.

6. PREDICTED SYSTEM PERFORMANCE

An instrument built according to the grating and slit farm specifications used here, if combined with a microchannel detector having the requisite field of view (40mm x 40 mm) and good spatial resolution (< 20um FWHM over its field) would deliver an unprecedented level of sensitivity, as detailed in Table 1. For this table we assume that the 16cm^2 of working field is 50% populated with open slits whose on/off pattern allows deconvolution with good efficiency. For high throughput, an f/5 acceptance cone is assumed; other focal ratios can be chosen to trade angular resolution and sensitivity. Another equally realistic and achievable example is presented in our companion paper[3].

TABLE 1: PREDICTED PROPERTIES, EUV CURVED-MULTISLIT SPECTROMETER

ETENDUE with 4cm x 4cm slit zone, 50% open area	
Open area of multislit, cm2	8
F/5 grating sky solid angle, steradians	0.04
Grating reflectance	0.4
Blaze efficiency	0.4
Detector QE	0.4
Filter transmission at 304	0.5
Effective Etendue, cm2.ster	0.010
OBSERVATION	
Observing time, seconds	1000
DETECTOR INTERNAL BACKGROUND	
Dark count rate c/cm2.sec	0.40
Dark count rate c/sec	3.2
Total background counts	3200
One sigma of background	57
HELIOPAUSE SIGNAL TO NOISE RATIO at 1 mR	
Intensity, ph/cm2.s.sr	80
Count rate, counts per second	0.80
Accumulated signal counts in one bin	800
Number of standard deviations	14

7. ALTERNATIVE SLIT AND DETECTOR LOCATIONS

The parameter space explored here, with α and γ near zero and β near 0.1 is not the only way to achieve a large corrected field using curved entrance slits. The symmetry of α and β seen in equations 2, 4, and 5 shows that the slits and detector can be exchanged without altering the slit geometry. Also, the traditional Eagle mounting for concave gratings has α and β equal, or nearly so; to avoid collision between the entrance slit and the detector, a nonzero value for γ is chosen. Eq. 5 shows that the Eagle geometry minimizes image rotation The resultant slits are straight in the center of the horizontal field, but curve towards each other on opposite sides of the center line.

8. VISIBLE WAVELENGTH DEMONSTRATOR

Here we illustrate the features of the curved-slit Rowland configuration using a visible demonstration spectrometer. The demonstrator was designed to have nearly identical optical performance to that of the desired 30.4 nm spectrometer appropriate for heliospheric He+ Doppler spectroscopy. The visible and the theoretical 30.4 nm spectrometers use nearly identical optical mountings, i.e. they both use a similar wavelength - groove spacing product, Rowland circle size and incidence angles. Both are designed to achieve a similar spectral resolution using the same large slit angular height and field width. The goal of this exercise is to validate the EUV spectrometer concept.

The visible demonstrator uses a conventional spherically concave diffraction grating ruled with 600 grooves/mm in an f/10 mount working near normal incidence. The grating radius was 750mm and the spectrometer was illuminated by a

sodium lamp; the spectra of interest was the sodium doublet lines at 589.0 and 589.6 nm. Interchangeable optical slit patterns were created using high-resolution Kodak film, featuring 20 um wide slits in a 40mm wide by 45mm high area. Each slit was curved in the film plane to compensate for astigmatic errors as described earlier, and the slit pattern was held in a cylindrically curved (R = 197 mm) mount to provide a flat detector field. The detector was a commercial CCD camera (PixeLink PL-A741) whose 8.6 x 6.9mm format of 1280 x 1024 pixels provided sufficient resolution to show the spectral line width over any selected small portion of the 40mm x 45mm image. Computer-driven stages allowed the slit assembly to be correctly positioned and the CCD camera to be focused and then translated to various locations within the planar image field. A representative half-field spectral image of the sodium doublet using our curved slit prescription and built up from nine subframe CCD images is shown in Figure 4 (right side). For comparison, the spectral image from a conventional straight slit is shown in Fig 4 (left side). It is evident that curving the slit compensates for the blur caused by a rotated astigmatic image, resulting in a well-resolved spectra even at large slit heights. The measured spectral resolving power of the curved slit image is >6000 over the entire length of the slit, as determined from direct profilometry. Figures 5, 6, and 7 show the deconvolution process described by Gruntman et al[3] and demonstrate that a resolving power of about 6000 is achieved in practice.

Figure 4 (above): Sodium doublet spectrum CCD images taken with a single straight slit (left) vs. single curved slit (right). Doublet wavelengths are 589.0 and 589.6 nm.

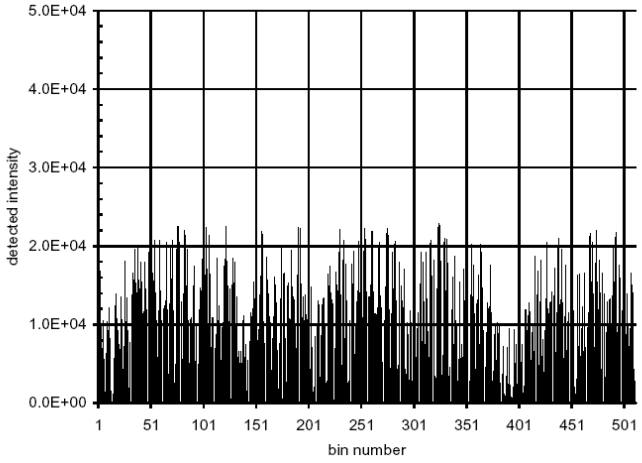

Figure 5 (above): Raw image histogram taken with 512 curved slits. Variations with bin number are primarily due to the random binary code pattern of the slits.

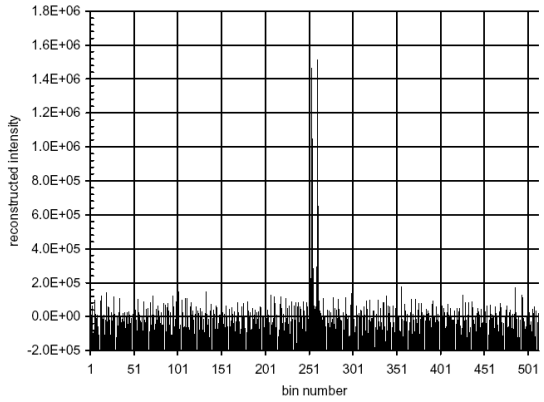

Figure 6 (above) Image deconvolved as described by Gruntman et al[3]. Each bin = 0.1 nm and the spectral range covered is 51 nm.

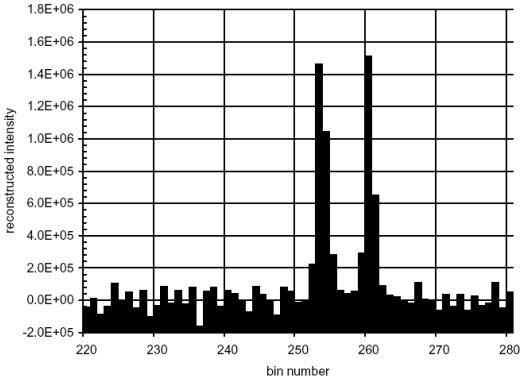

Figure 7 (above) Image deconvolved and magnified to show the details of the sodium line doublet. Resolution is about 0.1nm; resolving power is therefore about 6000.

9. APPLICATIONS TO ASTRONOMY AND SPACE PHYSICS

The motive for this study has been to probe the He+ ion dynamics of the expanding solar wind and to discover its termination shock by virtue of the characteristic signature of the Doppler structure in emission spectrum. Such a measurement drives all three constraints: resolving power of a few thousand, sensitivity at the milliRayleigh level for exposures of 1ks duration, and limited instrument size and mass. We have demonstrated a new spectrometer configuration that provides an unprecedented combination of diffuse sensitivity, spectral resolution, and compactness. The curved-multislit Rowland spectrometer may have a variety of other applications in which these same requirements are encountered, such as, for example, in studies of planetary environments (upper atmospheres, ionospheres, and magnetospheres).

ACKNOWLEDGMENT

The authors gratefully acknowledge the support from NASA contract NAG5-12779.

REFERENCES

1. M. Gruntman, "Imaging the three-dimensional solar wind," J. Geophys. Res. **106,** 8205 (2001).

2. M.Gruntman, "Mapping the Heliopause in EUV," Proc. EUV Colloquium, COSPAR (2001).

3. M.Gruntman, M.Lampton, J.Edelstein "Imaging three-dimensional heliosphere in EUV," Proc. SPIE 5901 #3, (2005).

4. H.A.Rowland "On concave gratings for optical purposes," Philos. Mag. **16**, 197 (1883).

5. H.G.Beutler, "The Theory of the Concave Grating," J. Opt. Soc. Am. **35**, 311 (1945).

6. T.Namioka "Theory of the concave grating, I" J. Opt. Soc. Am. **49**, 446 (1959); II, J. Opt. Soc. Am. **49**, 460 (1959); III, J. Opt. Soc. Am. **49**, 951 (1959).

7. G.H.Spencer and M.V.R.K.Murty, "General Ray-Tracing Procedure," J. Opt. Soc. Am. **52**, 672 (1962).

8. M.Neviere, D.Maystre, and W.R.Hunter "On the use of classical and conical diffraction mountings for XUV gratings," J. Opt. Soc. Am. **68,** 1106 (1978).

9. M. Sholl, B. Donakowski, G. Gaines, M. Lampton, M.Hurwitz, M.M. Sirk, E.Taylor "Optics design and performance for the Cosmic Hot Interstellar Plasma Spectrometer (CHIPS)," Proc. SPIE **5164** (2003).

10. S.Habraken, C.A.Jamar, P.Rochus, S.Mende, and M.Lampton "Optical design of the FUV spectrographic imager for the IMAGE mission," Proc. SPIE **3114,** 544 (1997).

11. S. Mende et al "Far ultraviolet imaging from the IMAGE spacecraft: 3. Spectral imaging of Lyman alpha and OI 135.6nm," Sp. Sci.Rev. **91,** 287 (2000).

12. M.Lampton, "Damping-undamping strategies for the Levenberg-Marquardt nonlinear least-squares method" Computers in Phys. **11,** 110 (1997).